










Early diagnosis and treatment of Alzheimer's disease by targeting toxic soluble A β oligomers

Maram Habashi^{a,1}, Suresh Vutla^{b,1}, Kuldeep Tripathi^{a,1} , Sudipta Senapati^{a,1} , Pradeep S. Chauhan^b, Anat Haviv-Chesner^a, Michal Richman^a, Samia-Ait Mohand^c, Véronique Dumulon-Perreault^d, Ramakotiah Mulamreddy^b , Eitan Okun^e , Jordan H. Chill^a , Brigitte Guérin^{c,d,2}, William D. Lubell^{b,2} , and Shai Rahimpour^{a,2} 

Edited by Lila Gierasch, University of Massachusetts Amherst, Amherst, MA; received June 22, 2022; accepted October 20, 2022

Transient soluble oligomers of amyloid- β (A β) are toxic and accumulate early prior to insoluble plaque formation and cognitive impairment in Alzheimer's disease (AD). Synthetic cyclic D,L- α -peptides (e.g., 1) self-assemble into cross β -sheet nanotubes, react with early A β species (1-3 mers), and inhibit A β aggregation and toxicity in stoichiometric concentrations, in vitro. Employing a semicarbazide as an aza-glycine residue with an extra hydrogen-bond donor to tune nanotube assembly and amyloid engagement, [azaGly⁶]-1 inhibited A β aggregation and toxicity at substoichiometric concentrations. High-resolution NMR studies revealed dynamic interactions between [azaGly⁶]-1 and A β 42 residues F19 and F20, which are pivotal for early dimerization and aggregation. In an AD mouse model, brain positron emission tomography (PET) imaging using stable ⁶⁴Cu-labeled (aza)peptide tracers gave unprecedented early amyloid detection in 44-d presymptomatic animals. No tracer accumulation was detected in the cortex and hippocampus of 44-d-old 5xFAD mice; instead, intense PET signal was observed in the thalamus, from where A β oligomers may spread to other brain parts with disease progression. Compared with standard ¹¹C-labeled Pittsburgh compound-B (¹¹C-PIB), which binds specifically fibrillar A β plaques, ⁶⁴Cu-labeled (aza)peptide gave superior contrast and uptake in young mouse brain correlating with A β oligomer levels. Effectively crossing the blood-brain barrier (BBB), peptide 1 and [azaGly⁶]-1 reduced A β oligomer levels, prolonged lifespan of AD transgenic *Caenorhabditis elegans*, and abated memory and behavioral deficits in nematode and murine AD models. Cyclic (aza)peptides offer novel promise for early AD diagnosis and therapy.

Alzheimer's disease | soluble A β oligomers | early diagnosis and therapy | PET imaging | cyclic D,L- α -(aza)peptide

Supramolecular interactions among β -sheets are vital for protein folding, recognition, and aggregation (1, 2). β -Sheet aggregation between amyloidogenic proteins is characteristic of the pathology of many diseases including prion and neurodegenerative conditions, such as Alzheimer's and Parkinson's diseases (AD and PD), which have foreboding socio-economic consequences (3–6). In AD, the polypeptides amyloid- β (A β) and tau misfold, oligomerize, and form toxic soluble oligomers and fibrils that accumulate in the brain in pathogenic pathways leading to synaptic loss and selective neuronal cell death (3, 5, 7).

Convincing evidence indicates A β aggregation and plaque accumulation occur early as determinant events in the brain leading to AD (8, 9). During the aggregation process, soluble oligomers of A β are suspected to be more deleterious than A β fibrils and plaques (10–13). Insight into factors promoting and disrupting β -sheets is critical for understanding the structural basis of amyloid pathology to create tools for early detection and effective treatment.

A quarter of a century of research to target soluble and fibrillar forms of A β has led to limited efficacy in clinical studies (14, 15). Inherent in the lack of success has been the inability to diagnose early A β species and late treatment of patients after significant brain damage has occurred. Recently, two monoclonal antibodies targeting A β oligomers have shown encouraging therapeutic efficacy in phase III clinical studies, and the antibody Aducanumab has received US Food and Drug Administration (FDA) approval (16–18).

Early diagnosis of AD by targeting A β oligomers, which precede those of tau, is critical for improving timely detection and therapeutic outcome (12, 19–21). Current methods of choice for monitoring AD are based on positron emission tomography (PET)/computed tomography (CT) imaging using FDA approved ¹⁸F-radiotracers, including AmyvidTM (¹⁸F-florbetapir), VizamyTM (¹⁸F-flutemetamol), NeuraceqTM (¹⁸F-florbetaben), and TauvidTM (¹⁸F-flortaucipir). Limited to adult patients suffering already from cognitive impairment, the former ¹⁸F-radiotracers, as well as the well-studied radiotracer ¹¹C-Pittsburgh compound B (¹¹C-PIB), all assess preferentially fibrils and insoluble plaques, and TauvidTM detects tau neurofibrillary tangle density and distribution (22–25). None detect soluble A β oligomers.

Significance

Alzheimer's disease (AD) associates closely with misfolding and aggregation of A β protein. Inability to detect early A β aggregates at presymptomatic stages has limited efforts to diagnose and treat AD. Employing a theranostic approach, neurotoxic A β oligomers were imaged by self-assembled cyclic D,L- α -(aza)peptide nanotubes in a presymptomatic transgenic mouse model. PET imaging with azapeptide radiotracers detected early A β oligomer in the thalamus prior to the spread of A β aggregates and fibrils to other brain parts. Treatment with therapeutic (aza)peptides mitigated deficits in behavior, cognition, memory, and learning in nematode and murine AD models.

Author contributions: K.T., S.S., A.H.-C., S.-A.M., V.D.-P., R.M., E.O., J.H.C., B.G., W.D.L., and S.R. designed research; M.H., S.V., K.T., S.S., P.S.C., A.H.-C., M.R., S.-A.M., V.D.-P., R.M., and J.H.C. performed research; M.H., S.V., K.T., S.S., P.S.C., A.H.-C., S.-A.M., V.D.-P., R.M., E.O., J.H.C., B.G., W.D.L., and S.R. analyzed data; and J.H.C., B.G., W.D.L., and S.R. wrote the paper.

The authors declare no competing interest.

This article is a PNAS Direct Submission.

Copyright © 2022 the Author(s). Published by PNAS. This open access article is distributed under Creative Commons Attribution-NonCommercial-NoDerivatives License 4.0 (CC BY-NC-ND).

¹M.H., S.V., K.T., and S.S. contributed equally to this work.

²To whom correspondence may be addressed. Email: Brigitte.Guerin2@USherbrooke.ca, william.lubell@umontreal.ca, or rahimis@biu.ac.il.

This article contains supporting information online at <https://www.pnas.org/lookup/suppl/doi:10.1073/pnas.2210766119/-/DCSupplemental>.

Published November 28, 2022.

Probes for detecting early A β oligomers in vivo are rare and mostly rely on fluorescence imaging (26–28). PET imaging has shown promise in relatively aged transgenic mouse models with established A β plaque pathology and apparent symptoms. For example, increased uptake compared with ^{11}C -PIB was achieved with an ^{124}I -labeled conjugate of a F(ab') $_2$ fragment of humanized oligomer-specific mAb158 and transferrin receptor antibodies, which revealed a different A β distribution in the cortical regions of transgenic ArcSwe mice relative to wild-type (WT) littermates (29, 30). Magnetic resonance imaging (MRI) signals were observed in the hippocampus and cortex of 5xFAD mice using a conjugate between oligomer-specific antibody NU-4 and magnetic nanostructures, which crossed the blood–brain barrier (BBB) upon intranasal administration (31, 32). For improved patient selection and accurate monitoring of response to treatment, a PET/CT imaging agent targeting soluble A β oligomers is acutely needed for early AD diagnosis (22).

Cross interactions between different amyloidogenic proteins are likely due to structural and functional similarities, which inspire the design of molecules that bind and modulate amyloid aggregation (33–36). Cyclic D,L- α -peptides comprised of even numbers of alternating D- and L- α -amino acids (e.g., **1**, *c*-[Lys 1 -D-Leu 2 -Nle 3 -D-Trp 4 -His 5 -D-Ser 6], Fig. 1) self-assemble into nanotube structures that replicate the intermolecular hydrogen-bonding patterns of cross β -sheets with features of amyloid proteins such as interstrand distances of 4.8 Å (Fig. 1 *A* and *B*) (37). The conformational antibody A11 recognizes the structural similarity of peptide **1** and toxic oligomers of various amyloidogenic proteins (38). At and above stoichiometric concentrations, peptide **1** was shown to engage soluble and low molecular weight A β species,

modulate aggregation, disassemble fibrils, and inhibit cell toxicity by an “off-pathway” mechanism (38, 39). Peptide **1** also bound other aggregation-prone polypeptides including PD-associated α -synuclein (α -syn) and tau-derived hexapeptide AcPHF6 (40, 41). Structure–activity relationship (SAR) studies of peptide **1** correlated antiamyloidogenic activity with self-assembly, both of which were diminished on replacement of D-Trp 4 with D-Ala 4 and on introduction of backbone *N*-methyl amide groups, respectively (38, 41). In addition, linear peptide counterpart failed to induce appreciable antiamyloidogenic activity (38, 39, 41).

On the hypothesis that equilibria between self-aggregated and dissociative states of cyclic D,L- α -peptides mediate the ability to engage and disrupt amyloid oligomers, aza-glycine (azaGly) analogs **2–7** of peptide **1** were synthesized to modulate self-assembly and probe effects on A β aggregation and toxicity (Fig. 1 *C*). In collagen model peptides, the Gly to azaGly switch added extra hydrogen-bond donors that enhanced triple helix stability (42). By replacing systematically each residue in peptide **1** with azaGly, self-aggregation and A β engagement were tuned using extra hydrogen bonds. Notably, at substoichiometric concentrations, [azaGly 6]-**1** (**7**) interacted with F19 and F20 residues in A β 42 monomers as indicated by high-resolution NMR studies, inhibited A β aggregation in thioflavin T (ThT) fluorescence assays, and improved rat pheochromocytoma PC12 cell viability. Targeting oligomeric forms of A β , ^{64}Cu -radiolabeled analogs of **1** and **7** detected early A β species with unprecedented sensitivity in PET imaging studies of 44-d-old young presymptomatic transgenic AD mouse model brains. In transgenic *Caenorhabditis* (*C.*) *elegans* AD models in vivo, peptide **1** and [azaGly 6]-**1** (**7**) decreased A β -induced toxicity and improved memory-associated functions by reducing

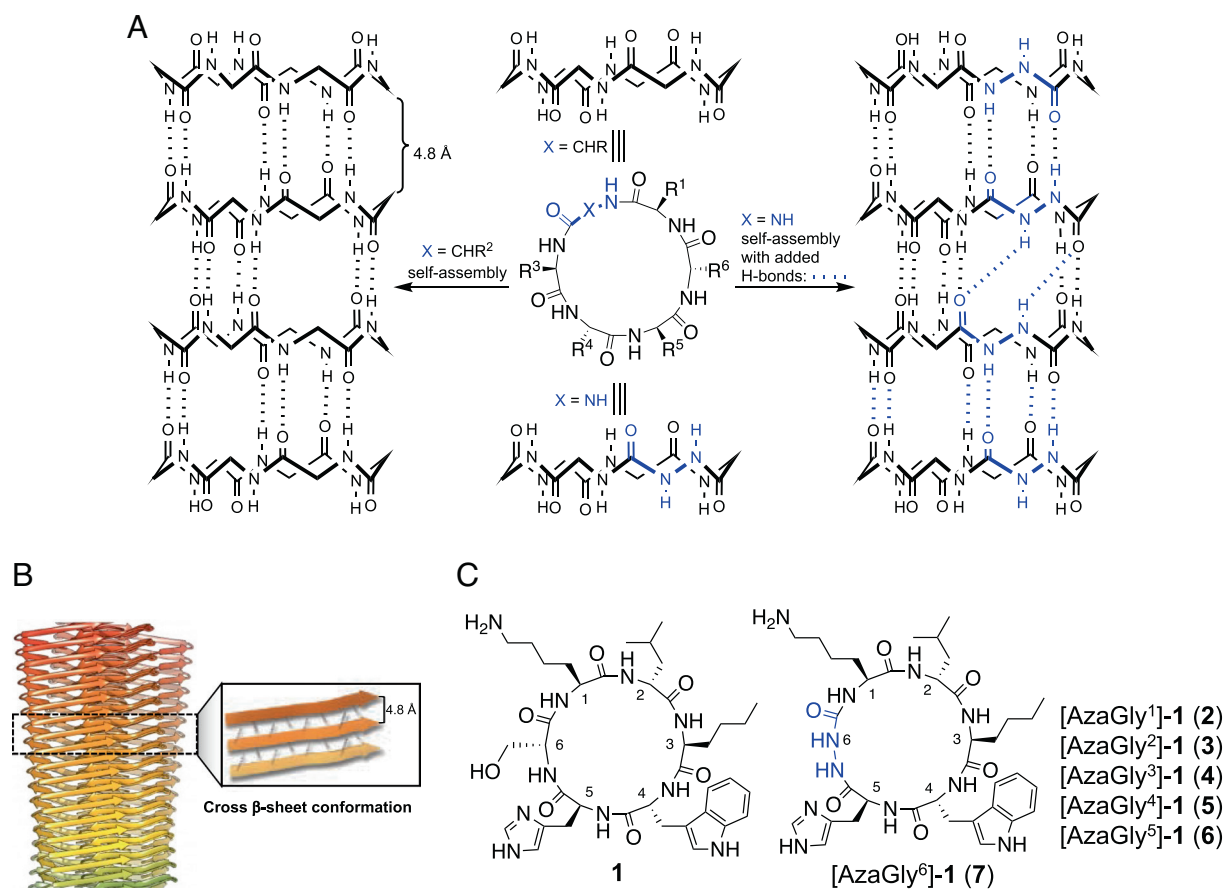


Fig. 1. (A) Potential influence of azaGly residue on hydrogen-bonding of cyclic D,L- α -hexapeptide nanotubes which share common cross β -sheet structures with (B) A β . For clarity, all side chains have been omitted. (C) Structures of cyclic D,L- α -peptide **1** and azaGly-cyclopeptides (**2–7**).

the amount of toxic A β oligomers. Furthermore, peptide **1** reversed AD pathological behaviors in a transgenic AD mouse model. Toward a new paradigm for early AD diagnosis and therapy, (aza)peptides **1** and **7** and their ^{64}Cu -radiolabeled analogs offer promising serum stability, clearance, and biodistribution profile.

Results

Effects of AzaGly Cyclic Peptides on A β Aggregation. All six possible [azaGly]-**1** analogs were made by the solid-phase synthesis and cyclization of linear precursors, purified on reverse-phase high-performance liquid chromatography (HPLC), and characterized (See *SI Appendix, Materials and Methods* section, *SI Appendix, Scheme S1* and *Table S1*). The ability of (aza)peptides **1-7** to disrupt A β 40 aggregation was measured using ThT, which emits fluorescence upon binding to amyloid fibrils (*SI Appendix, Table S2*) (43). Aggregation of A β was, respectively, inhibited with similar (**3**, **4**, and **6**) and significantly higher (**2**, **5**, and **7**) activity by the azaGly analogs compared with peptide **1** (Fig. 2 and *SI Appendix, Fig. S1* and *Table S2*). At 1:0.1 A β :peptide molar ratios at which parent peptide **1** was inactive, [azaGly⁶]-**1** (**7**) inhibited by 73% and 75% the aggregation of A β 40 and A β 42, the latter being relevant to AD pathology (Fig. 2 *B* and *C*). Reduced aggregation of A β 40 was also observed at 1:0.1 A β :peptide molar ratios using [azaGly¹]-**1** (**2**) and [azaGly⁴]-**1** (**5**) (*SI Appendix, Fig. S1 B and F* and *Table S2*). Azapeptide **2** increased however A β 40 aggregation at 1:10 A β :peptide molar ratio, likely due to self-assembly of **2** at 100 μM into fibrils, that may seed A β 40 aggregation (*SI Appendix, Fig. S1 C*). At low A β :peptide ratios, azaGly peptides **2**, **5**, and **7** prolonged generally the aggregation lag phase, suggesting interaction and inhibition of early A β species (*SI Appendix, Fig. S1*).

Transmission electron microscopy (TEM) indicated self-assembly of azapeptides **2** and **7** at high concentrations into unbranched long fibrils with similar characteristics as the nanotubes of parent peptide

1 (Fig. 2*G* and *SI Appendix, Fig. S2*) (38). Azapeptide **5** did not aggregate under these conditions. The TEM image of untreated A β after aging for 72 h exhibited dense long unbranched fibrils (Fig. 2*D*), but no fibrils were observed on exposure of A β to [azaGly⁶]-**1** (**7**) even at substoichiometric concentrations (1:0.1 A β :peptide) (Fig. 2*F*), at which azapeptide **7** did not self-assemble (Fig. 2*H*). Similarly, azapeptide **5** abolished the formation of A β fibrils at a 1:5 ratio A β :peptide molar ratios (*SI Appendix, Fig. S2 F*). Large fibrils were observed from A β samples incubated with a fivefold excess of **2** (*SI Appendix Fig. S2 E*). Consistent with the ThT assays (*SI Appendix, Fig. S1* and Fig. 2*B*), TEM indicated that [azaGly⁴]-**1** (**5**) and [azaGly⁶]-**1** (**7**) modulated A β aggregation and morphology while excess of **2** promoted A β aggregation (*SI Appendix, Fig. S2 E*). Coherent with TEM imaging (Fig. 2 *G* and *H* and *SI Appendix, Fig. S2*), dynamic light scattering (DLS) experiments at increasing concentrations indicated self-assembly of azapeptides **2** and **7** occurred, respectively, at concentrations higher than 20 μM and 30 μM with 20-min and 60-min lag phases (*SI Appendix, Fig. S2 H-L*), and azapeptide **5** did not self-assemble. The effect of azapeptide **7** on A β 40 monomer was studied using DLS and photoinduced cross-linking of unmodified proteins (PICUP) combined with denaturing polyacrylamide gel electrophoresis (PAGE) (44). Over 72 h, A β 40 monomer amounts decreased significantly with the formation of large oligomers and fibrils (>300 nm, *SI Appendix, Fig. S3 A*). Incubation with [azaGly⁶]-**1** (**7**), preserved the amount of A β 40 monomers, and favored smaller at the expense of larger aggregates (*SI Appendix, Fig. S3 B*).

Dot-blot assays using conformation-dependent antibodies (OC and A11) differentiated the effects of [azaGly⁶]-**1** (**7**) on A β fibril and soluble toxic oligomer formation (34, 45). Fibrils and oligomers were, respectively, identified by OC and A11 antibodies at different time intervals during incubation of A β 40 alone and with fivefold concentrations of peptide **1** and azapeptide **7** (Fig. 2*I*). The reactivity of A β to both antibodies increases steadily over time, but after

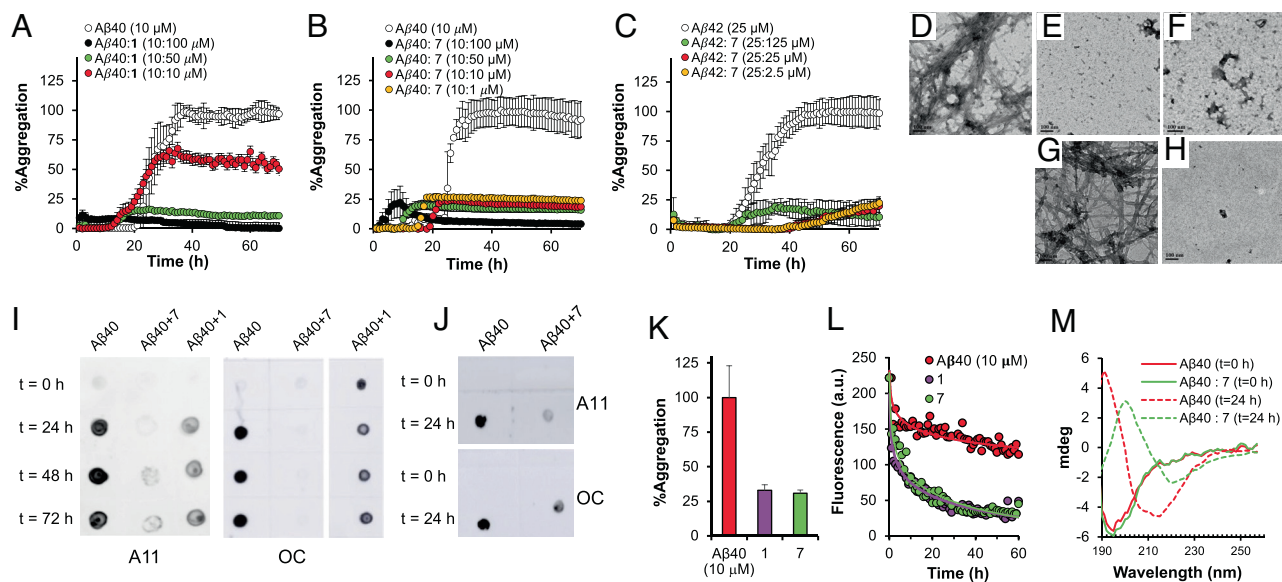


Fig. 2. Inhibitory activity of (aza)peptides **1** and **7** on A β aggregation. ThT fluorescence kinetics of A β 40 in the absence or presence of (A) **1** and (B) **7**. (C) Effect of **7** on aggregation of A β 42. Incubation of A β 40 (10 μM) and A β 42 (25 μM), respectively, without or with increasing concentrations of (aza)peptides was done at 37°C, and 100% aggregation was determined based on ThT fluorescence of A β alone. Experiments were carried out in triplicate. Data represent one out of the mean \pm SD of three experiments. TEM images after 72 h of (D) A β 40 (10 μM) alone; A β 40 treated with **7** at (E) 50 μM and (F) 1 μM ; **7** alone at (G) 50 μM and (H) 1 μM in PBS. Negatively stained samples are shown. Effects of **7** on A β 40 oligomer and fibril formation using oligomer- (A11: *I* Left and *J* Upper panels) and fibrillar-specific (OC: *I* Right and *J* Lower panels) antibodies. Monomeric A β 40 (30 μM) was aged up to 72 h alone and with (I) 150 μM of **1** and **7** or (J) 3 μM of **7**, spotted onto nitrocellulose membranes and probed with A11 and OC antibodies. Capability and kinetics of **7** to disassemble A β 40 fibrils. (K) Relative fluorescence intensity in ThT assays of 3-d-aged fibrillar A β 40 (10 μM) incubated for 24 h alone or with a fivefold excess of **1** or **7**. (L) A β 40 fibril disassembly rate with **1** and **7**. Results are the average \pm SD ($n = 3$ each) and representative of two experiments. (M) Effects of **7** on A β 40 secondary structure transition. Time dependent far-UV CD spectra of freshly prepared A β 40 monomer (10 μM) incubated alone and with substoichiometric concentration (0.1 μM) of **7** in phosphate buffer (50 mM, pH 7.4) after 0 h (full lines) and 24 h (dashed lines). Data are representative of two independent experiments.

48 h, decreases for A11 antibody, due to the conversion of soluble oligomer to fibrils (34, 38). Soluble toxic A β oligomer and fibril formation, both decreased more dramatically upon incubation with azapeptide 7 than with peptide 1 (Fig. 2 *I*, *Left* and *Right* panels). Moreover, azapeptide 7 decreased oligomer and fibril amounts at substoichiometric concentrations (Fig. 2*J*). In control experiments of (aza)peptide aged alone, only 1 reacted with A11 and OC antibodies at 150 μ M (*SI Appendix*, Fig. S4) (38).

Mature A β fibrils were disassembled in the presence of a fivefold excess of azapeptide 7 with similar kinetics as peptide 1 as indicated by loss of ThT fluorescence over time (Fig. 2 *K* and *L*). Disassembly of A β fibrils by azapeptide 7 did not generate toxic oligomers as indicated by decreased amounts of A11-reactive oligomers (*SI Appendix*, Fig. S5) (46, 47). In agreement with the ThT results (Fig. 2), azapeptide 7 reduced the amounts of OC-reactive A β fibrils (*SI Appendix*, Fig. S5). An equilibrium between fibrils that bind ThT and monomeric and soluble A β species may be shifted by preferential binding of azapeptide 7 to the latter. Alternatively, azapeptide 7 may remodel the fibrils into structures that do not bind OC antibody. Agents previously shown to strongly bind soluble forms of A β , such as antibodies and (-)-epigallocatechin gallate (EGCG) have interfered with aggregation and disaggregated preformed fibrils through recycling mechanisms (46, 48). The ensemble of immunochemical, ThT, and TEM data, all indicate that soluble oligomers and fibrils, both were reduced by [azaGly⁶]-1 (7) with greater effectiveness than peptide 1, due probably to stabilization of A β monomer and non-toxic early dimers and trimers (38).

Similar to conformation-specific antibodies which interact with multiple amyloids (34, 49), peptide 1 was previously shown to have a panamyloid selectivity and engaged and inhibited the aggregation and toxicity of different pathogenic amyloids: e.g., α -syn; tau-derived hexapeptide AcPHF6 (40, 41). Azapeptide 7 was shown to also bind other aggregation-prone proteins. In the ThT assay, [azaGly⁶]-1 (7) dose-dependently reduced the aggregation of α -syn at substoichiometric concentrations at which peptide 1 was inactive (*SI Appendix*, Fig. S6).

Effect of [azaGly⁶]-1 (7) on A β Conformation. Changes in the secondary structure of A β in the presence of azapeptide 7 were first studied using far-UV circular dichroism spectroscopy (far-UV CD, Fig. 2*M* and *SI Appendix*, Fig. S7). Over time, the CD curve shape of A β converts from a random coil with a negative maximum around 195 nm into an antiparallel β -sheet-rich secondary structure with positive and negative maximum, respectively, around 193 nm and 215 nm (Fig. 2*M*). The β -sheet curve magnitude was largely reduced on incubation of A β with a fivefold excess of azapeptide 7 (*SI Appendix*, Fig. S7*B*), correlating with diminished aggregation. The CD spectra of azapeptide 7 alone and in a 5:1 ratio with A β at $t = 0$ (*SI Appendix*, Fig. S7 *C* and *A*) exhibited a positive peak at 226 nm attributable to Trp–Trp interactions in a self-assembled nanotube (38, 50). After incubation with A β for 24 h, the peak disappeared indicating nanotube disassembly into monomeric and A β -engaged 7 (*SI Appendix*, Fig. S7*B*). In CD spectra of A β incubated with substoichiometric concentrations of azapeptide 7, the β -sheet curve magnitude was reduced, and a parallel β -sheet curve shape was formed with a positive maximum at 201 nm and a negative maximum at 221 nm (Fig. 2*M*). A similar shift from antiparallel to parallel β -sheet curve shape had previously been observed on treatment of A β with stoichiometric concentrations of peptide 1 (38).

The interactions between A β 42 monomers and azapeptide 7 were next examined using high-resolution NMR spectroscopy. The NMR experiments were performed at substoichiometric azapeptide concentration (0.1:1 mol:mol 7:A β 42 ratio) to mimic the ThT

and CD experiments (Fig. 3). Low concentration (20 μ M) and low temperature were maintained to avoid rapid A β 42 aggregation (for details see *SI Appendix*). The ¹H,¹⁵N-heteronuclear single quantum coherence (HSQC) technique was initially used to identify ligand-induced chemical shift changes and peak broadening in a fingerprint spectrum in which a single peak is observed per residue along the A β 42 backbone (*SI Appendix*, Fig. S8). Considering the importance of aromatic side chain interactions for early A β self-assembly and toxicity (51, 52), the influences of azapeptide 7 on the aromatic residues of A β 42 were next probed in the ¹H,¹³C-HSQC spectrum. Peaks were assigned in this typically poorly dispersed spectral region by observing nuclear overhauser effect spectroscopy (NOESY) (H β /H δ and H β /H ϵ) and total correlation spectroscopy (TOCSY) correlations (Fig. 3*B*).

Weak interactions were observed between the backbone amides of A β 42 and azapeptide 7 in the ¹H,¹⁵N-HSQC experiment (*SI Appendix*, Fig. S8*B*). Azapeptide-induced chemical shift changes were small, in the range of typical ¹H-normalized Euclidean perturbations of 3–8 Hz. Some line-broadening was observed, particularly at the C-terminal A β 42 residues, which exhibited a broadening trend consistent with the higher hydrophobicity in this region. The derivation of meaningful residue-specific information was however precluded by low S/N-levels due to sample concentration and pH. In contrast, pronounced azapeptide-induced changes were observed in the aromatic region of the ¹H,¹³C-HSQC spectrum. Peaks corresponding to residues F19 and F20 of the K¹⁶LVFF²⁰ aggregation motif of A β 42 disappeared in the presence of azapeptide 7 in the ¹H,¹³C-HSQC spectrum (Fig. 3 *C* and *D*). By interacting with residues F19 and F20 in the aggregation-prone region of A β 42, azapeptide 7 interferes with early intermolecular A β 42 contacts, which are important for aggregation and fibrilization processes (38, 51, 52).

[azaGly⁶]-1 (7) Inhibits A β -Mediated Cytotoxicity. Self-assembly and aggregation of A β are key components of AD-related pathogenesis. Ability to reduce A β -induced toxicity was tested in rat pheochromocytoma neuronal-like PC12 cells. Dot-blot analyses indicated that A11-reactive A β oligomers reached optimal levels when 20 μ M concentrations of A β were aged for 24 h (Fig. 2*I*). Therefore, A β was pretreated with and without peptide 1 and azapeptide 7 for 24 h and exposed further to PC12 cells for 48 h. Cell viability was assessed by the MTT assay, which is commonly used to determine A β toxicity (*SI Appendix*, Table S2 and Fig. 4*A*) (53, 54). Cell metabolism decreased to 68% in the presence of A β . At 1:5 A β :peptide ratios, both peptide 1 (88%) and [azaGly⁶]-1 (7, 93%) exhibited protective effects, which at 1:1 A β :peptide ratios were lost by peptide 1 (70%) and retained by azapeptide 7 (89%). Furthermore, 3 mol % of azapeptide 7 gave significant cell protection ($P < 0.05$) (Fig. 4*A*). No toxicity was exhibited by azapeptide 7 even at 100 μ M.

Azapeptide 7 Reduces A β Toxicity and Pathological Symptoms In Vivo by Decreasing A β Oligomer Levels. Azapeptide 7 was examined in three in vivo transgenic *C. elegans* models expressing human A β 42. The CL2006 *C. elegans* strain produces constitutively a body wall muscle-specific A β 42, the aggregation of which causes age-dependent paralysis, motility dysfunction, and consequently decreased lifespan (55). The CL2355 strain expresses a temperature-inducible panneuronal A β 42, which upon accumulation leads to deficits in chemotaxis, associative learning, and thrashing in liquid (56). The GMC101 strain is a temperature permissive strain that overexpresses human A β 42 in body wall muscle cells, which results in temperature-inducible paralysis (57). The CL2006 mutant and control CL802 WT worms had respective lifespans of 13.6 and 15.6

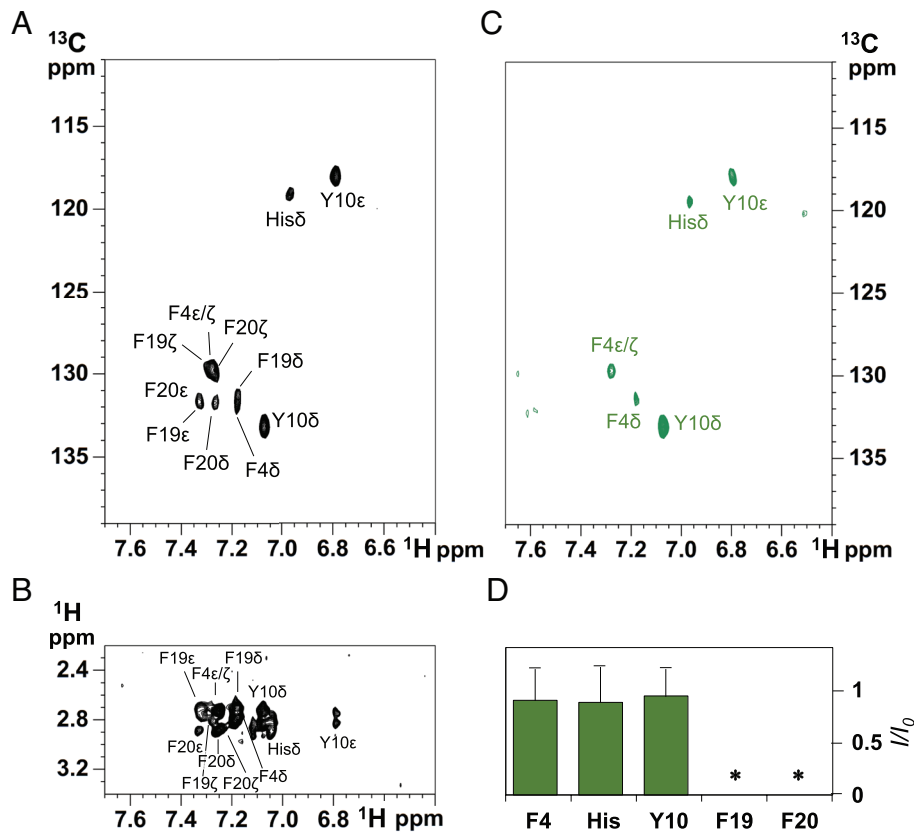


Fig. 3. NMR characterization of the Aβ₄₂ – azapeptide 7 interaction. (A) Annotated aromatic region of the ¹H,¹³C-HSQC spectrum of 20 μM Aβ₄₂ (in 95:5 H₂O: d₆-DMSO) with assignments based on the homonuclear NOESY. (B) The H^α/H^β region of the Aβ₄₀ homonuclear 2D NOESY spectrum acquired in ²H₂O used for assignment of the Aβ₄₂ aromatic region. Aβ₄₀ allows for higher sample concentrations without aggregation and exhibits identical aromatic signals in the NOESY spectrum, due to the presence of the relevant residues in the N-terminal portion of the sequence. Histidine H^β is slightly shifted due to a small pH change. (C) Same as (A) after addition of 2 μM of azapeptide 7. (D) Peak intensity ratios (I/I₀) for spectra with and without the azapeptide, calculated as an average over all protons of a given residue. An aggregate value is shown for overlapping H6/H13/H14. Asterisks denote that in the presence of azapeptide 7, F19 and F20 cross-peaks were undetectable above noise level.

d ($P < 0.001$, Fig. 4 B and C). Treatment of CL2006 worms with azapeptide 7 (50 μM) increased ($P < 0.0001$) lifespan to that of WT and negated the effect of overexpressed Aβ. Azapeptide 7 exhibited no toxicity and no influence on WT CL802 worm longevity (Fig. 4 B and C). Temperature-sensitive CL2355 mutants and WT CL2122 worms bend, respectively, about 61 and 73 times per min at an elevated temperature (23°C vs. 16°C) due to the former suffering from Aβ-induced toxicity ($P < 0.0001$, Fig. 4D). On feeding with increasing concentrations of azapeptide 7, CL2355 mutants exhibited dose-dependent increased motility to levels exhibited by untreated WT CL2122 (Fig. 4D). No effect on bending frequency was observed on treatment of WT CL2122 worms with azapeptide 7. Similar results were obtained when CL2355 strain was treated with peptide 1 (SI Appendix, Fig. S9A). Significant protective effects from paralysis were also observed on feeding the transgenic GMC101 strain peptide 1 and azapeptide 7 at 5 and 50 μM (SI Appendix, Fig. S10 A and B). No relation between the in vivo activity of peptide 1 and effects on Aβ synthesis was shown by the absence of difference in mRNA levels in treated and untreated worms using quantitative real-time PCR (qPCR) (SI Appendix, Fig. S10C).

In the chemotaxis assay, activation of several sensory neurons is required to stimulate the motor neurons (58). The chemotaxis indexes (CI) of the control CL2122 and transgenic CL2355 strains were, respectively, 0.29 ± 0.01 and 0.18 ± 0.01 , suggesting that the latter are neuronally impaired. Treatment of CL2355 mutants with (aza)peptides 1 and 7 dose dependently increased CI levels to that of the WT and neutralized the damaging effect of aggregated Aβ (Fig. 4E and SI Appendix, Fig. S9B). The CI levels of

WT CL2122 worms did not change on treatment with (aza)peptide 1 or 7. (Aza)peptides 1 and 7 demonstrated a significant protective effect on the pathological behaviors of the transgenic strains even at low micromolar concentrations (Fig. 4 D and E and SI Appendix, Figs. S9 and 10). In control experiments, the linear analog of peptide 1 (H-D-Leu-Nle-D-Trp-His-D-Ser-Lys-OH; Lin-1) and cyclic D,L-α-peptide [w4a]-1 [*c*-(D-Leu-Nle-D-Ala-His-D-Ser-Lys)] that self-assembled only at high concentrations and failed to inhibit Aβ aggregation in vitro (39), both were significantly less protective than peptide 1 in AD transgenic *C. elegans* CL2355 (SI Appendix, Fig. S9).

Immunochemical dot-blot analysis of equal amounts of extracted proteins from CL2006 mutants indicated that azapeptide 7 reduced the overall levels of Aβ with more pronounced effects on A11-reactive oligomers (Fig. 4F). Western blot analysis of extracted proteins from azapeptide-treated CL2006 animals demonstrated a clear decrease in Aβ hexamers (~27 Kd) and trimers (~14 Kd) (Fig. 4 G and H). Hexamers of Aβ have been suggested to be building blocks for toxic aggregates, including Aβ-derived diffusible ligands, Aβ dodecamer, and globulomers (44, 59, 60). Aβ hexamers were also shown to organize into β-barrel-shaped structures associated with pore-induced toxicity (61, 62). The decrease in Aβ trimers and hexamers induced by azapeptide 7 was concomitant with an increase in soluble Aβ dimer levels (~8.5 Kd) (Fig. 4G). Stabilization of dimers was shown by PICUP experiments to inhibit Aβ aggregation and toxicity (38). Consequently, the number of Aβ plaques in the head region of CL2006 mutants fed with azapeptide 7 were reduced compared with those of vehicle-treated worms as indicated

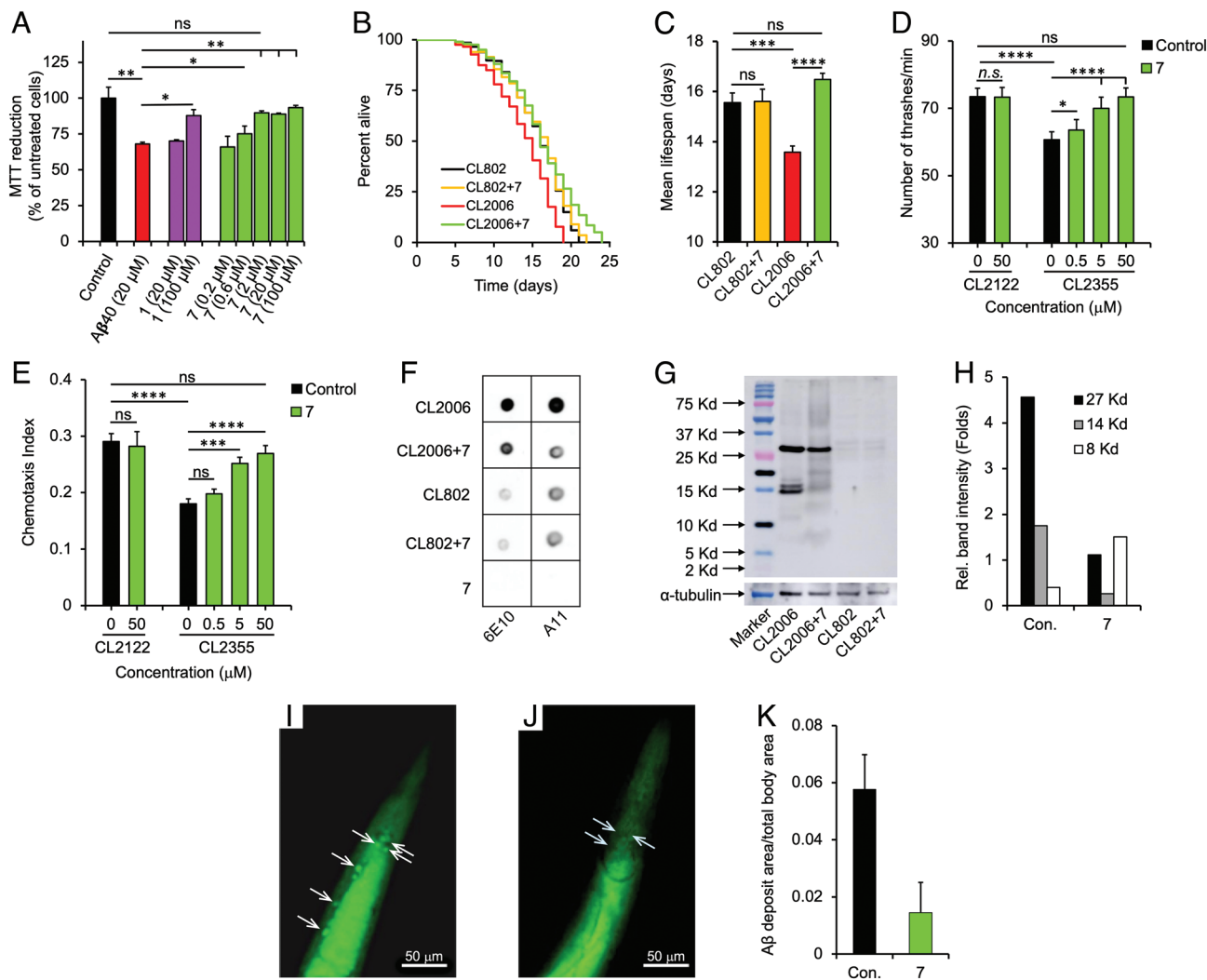


Fig. 4. Effects of peptide **1** and azapeptide **7** on A β -mediated toxicity in PC12 cells and in vivo in transgenic *C. elegans* models. (A) A β 40 (20 μ M) was aged for 48 h alone or with increasing concentrations of **1** and **7**, exposed to PC12 cells for 24 h and cell viability was determined by the MTT assay. Results are expressed as a percentage of the control (untreated) cells and are reported as mean \pm SD from three assays and analyzed by a one-way ANOVA followed by Tukey's multiple comparison test ($n = 3$ each; $*P < 0.05$, and $**P < 0.01$). (B) Kaplan–Meier survival plots and (C) median lifespan of transgenic CL2006 and WT CL802 strains treated with **7** (50 μ M) or vehicle (5% DMSO) reported as mean \pm SD from three experiments and were analyzed by a one-way ANOVA followed by Tukey's multiple comparison test ($n = 25$ each; $***P < 0.001$, $****P < 0.0001$, ns = not significant). (D) Effect of **7** on motility of *C. elegans* models. Transgenic CL2355 and control CL2122 worms were fed increasing concentrations of **7** at 16°C for 36 h and then at 23°C for another 36 h, before the number of thrashes were counted for 1 min. Data are plotted as a mean \pm SD from three experiments and were analyzed by a one-way ANOVA followed by Tukey's multiple comparison test ($n = 20$, each; $*P < 0.05$, and $****P < 0.0001$, ns = not significant). (E) Chemotaxis behavior of neuronal A β -expressing strain *C. elegans* CL2355 and transgenic control strain CL2122 in the absence or presence of **7**. Worms were fed increasing concentrations of **7** at 16°C for 36 h and then at 23°C for another 36 h. At the end of the incubation time, the animals were placed in the center of an assay plate (100 \times 15 mm) containing 1 μ L of attractant (0.1% benzaldehyde in ethanol) and 1 μ L 1 M sodium azide at two opposite edges of the plate, and 1 μ L 1 M sodium azide on the remaining opposite edges of the plate. The chemotactic index (CI) was then determined after 1-h incubation at room temperature, using the formula: CI = (number of worms at attractant sites - number of worms at control sites)/total number of worms. Results are reported as mean \pm SD from three independent experiments and were analyzed by a one-way ANOVA followed by Tukey's multiple comparison test ($n = 20$ each; $***P < 0.0005$, $****P < 0.0001$, ns = not significant). (F) Representative dot-blot analysis of equal amounts of the proteins extracted from *C. elegans* CL2006 and CL802 strains fed **7** or vehicle, after probing with sequence-specific 6E10 and oligomer-specific A11 antibodies. (G) Representative western blot (WB) analysis of A β species in the transgenic *C. elegans* CL2006 and the control CL802 fed with or without **7**. Equal amounts of extracted proteins were loaded onto each gel lane and immunoblotted with an anti-A β antibody (6E10) or α -tubulin. (H) Quantification using ImageJ software of A β oligomers (the bands at 14 and 27 kDa) in CL2006 and CL802 worms fed either vehicle or **7**. Representative images of A β deposits (shown as white arrows) in transgenic *C. elegans* CL2006 fed (I) without or (J) with **7** obtained by thioflavin S staining. (K) Quantitative analysis using ImageJ of A β deposits in (I) and (J). The quantity is expressed as mean number \pm SD of A β deposit area per total examined area of the worm ($n = 3$ for each analysis).

by staining with thioflavin S and fluorescent microscopy imaging (Fig. 4 I–K). In total, the immunochemical results indicated that azapeptide **7** alleviated AD pathology by reducing both A β oligomer and plaque levels.

Azapeptide Fibrils Are Not Pathogenic Seeds. Azapeptide **2** was collectively shown to effectively generate fibrils by ThT, TEM, and DLS studies (SI Appendix, Figs. S1 and S2). The inability of [azaGly¹]-**1** (**2**) to seed the pathogenic aggregation and toxicity of A β was shown by in vitro and in vivo experiments. In dot-blot

experiments, a fivefold excess of azapeptide **2** (150 μ M) acted like [azaGly⁶]-**1** (**7**) and reduced A11 antibody reactivity toward the A β -azapeptide complex (SI Appendix, Fig. S11A). In an orthogonal experiment analogous to cellular assays to assess self-propagating conformers (63), transgenic *C. elegans* CL2006 were, respectively, fed high concentrations of monomeric ($t = 0$) and aged ($t = 20$ h) fibrillar azapeptide **2** (30 μ M), neither of which increased the number of ThS-positive A β plaques (SI Appendix, Fig. S11 B–E). Furthermore, egg laying rates, which are indicative of toxicity, in transgenic *C. elegans* CL2006 and wild-type control CL802 strains

were observed to be unchanged on feeding worms monomeric or fibrillar azapeptide **2** (*SI Appendix, Fig. S11F*). In addition, dot-blot studies of the proteins extracted from GMC101 transgenic *C. elegans* treated with [azaGly¹]-**1** (**2**) and analyzed by A11 and OC antibodies were observed to be the same as that of untreated GMC101 worms (*SI Appendix, Fig. S11G*) confirming that neither monomeric nor aggregated azapeptide **2** was pathogenic.

Biostability and Biodistribution of ⁶⁴Cu-Radiolabeled Conjugates of **1 and **7**.** Metal radiotracers exhibit beneficial properties, such as long half-life, facile late-stage radiolabeling, and potential utility for theranostic applications. The ⁶⁴Cu²⁺ radionuclide emits β⁺ particles with a half-life (t_{1/2}) of 12.7 h enabling noninvasive and sensitive PET imaging studies in the brain. The ⁶⁴Cu-radiolabeled conjugates of (aza)peptides **1** and **7** were synthesized and shown to serve as biostable and bioavailable tracers of Aβ in WT and 5xFAD transgenic AD mice. 2,2',2''-(1,4,7-triazacyclononane-1,4,7-triyl)triacetic acid (NOTA) was selected as a metal chelator with high ⁶⁴Cu affinity and resistance to transmetalation (64). The thermodynamic stability constants of Cu²⁺ complexes [log K_{ML}, in which the metal (M) is Cu²⁺ and the ligand (L) is either Aβ or NOTA at pH 7.4] of Aβ and NOTA have, respectively, been reported to be 10.38 (65, 66) and 23.33 (67); hence, transchelation of ⁶⁴Cu²⁺ from NOTA in the presence of Aβ should not be significant. Conjugation of NOTA to the lysine ε-amine provided, respectively, [Lys¹(NOTA)]-**1** (**8**) and [Lys¹(NOTA), azaGly⁶]-**1** (**9**), which were analyzed by mass spectrometry and purified to homogeneity by HPLC (*SI Appendix, Scheme S2*). Attachment of NOTA to peptide **1** enhanced antiamyloidogenic and cytoprotective activity in the ThT and MTT assays (*SI Appendix, Table S2*). Relative to [azaGly⁶]-**1** (**7**), [Lys¹(NOTA), azaGly⁶]-**1** (**9**) had reduced antiamyloidogenic activity but retained the ability to reverse completely the pathological effect of Aβ in PC12 cells at a fivefold excess (*SI Appendix, Table S2*).

Radiolabeling of [Lys¹(NOTA)]-**1** (**8**) and [Lys¹(NOTA), azaGly⁶]-**1** (**9**) was, respectively, performed using ⁶⁴Cu(OAc)₂ in yields superior to 95% giving high specific molar activities (66–72 TBq/mmol). The ⁶⁴Cu-radiolabeled conjugates ⁶⁴Cu-**8** and ⁶⁴Cu-**9** exhibited high stability in plasma (*SI Appendix, Fig. S12*). Plasma proteins bound, respectively, 81% and 26% of all ⁶⁴Cu from ⁶⁴Cu-radiolabeled ⁶⁴Cu-**8** and ⁶⁴Cu-**9**. Only 6.6% and no trace of free ⁶⁴Cu were detected after 24 h in the supernatant fractions following plasma incubation with **8** and **9** and precipitation (*SI Appendix, Fig. S12*).

For biodistribution studies, WT mice were injected intravenously with ⁶⁴Cu-radiolabeled conjugates. The animals were perfused with saline 20 h post injection, prior to dissection of tissues to examine uptake of radiolabeled conjugates (*SI Appendix, Table S3*). Both analogs penetrated equally the BBB of the WT mice. Lower accumulation of [Lys¹(⁶⁴Cu/NOTA), azaGly⁶]-**1** (⁶⁴Cu-**9**) was detected in liver, spleen, and lungs compared with [Lys¹(⁶⁴Cu/NOTA)]-**1** (⁶⁴Cu-**8**).

PET/CT Imaging of Aβ Pathology in Transgenic Mice. Brain accumulation and ability to detect Aβ species were tested in 5xFAD transgenic mice that develop rapidly severe amyloid pathology as a result of the presence of the Swedish (K670N/M671L), Florida (I716V), and London (V717I) mutations in Amyloid Precursor Protein (APP), and the M146L and L286V mutations in Presenilin-1 genes (68). The 5xFAD model is advantageous for studies of early amyloid deposition. Around 1.5 mo of age, the 5xFAD model has been reported to exhibit accumulation of intraneuronal Aβ₄₂ levels in the cortex, the hippocampus, and the thalamus. Extracellular amyloid deposition can be detected

around 2 mo and increases with age. Initial memory impairment is observed between 4 mo and 5 mo of age (68).

In 6-mo-old 5xFAD mice injected with ⁶⁴Cu-**8** and ⁶⁴Cu-**9**, PET imaging showed high hippocampal and cortical uptake in the brains of AD mice (*SI Appendix, Fig. S13*). In head-to-head comparisons, PET imaging of ⁶⁴Cu-**9** showed fivefold higher hippocampal uptake relative to ⁶⁴Cu-**8** (2.03 ± 0.06 vs. 0.43 ± 0.01 %ID/g), which correlated with the better activity of azapeptide **7** compared with peptide **1** in in vitro experiments. Moreover, uptake of ⁶⁴Cu-**9** in the hippocampus (1.285 ± 0.034 %ID/g) was similar to that of the well-studied Aβ imaging agent ¹¹C-Pittsburgh compound B (¹¹C-PIB; 1.038 ± 0.028 %ID/g) at 1 h post injection, but twofold higher (2.03 ± 0.06) with better contrast at 20 h post injection. PET imaging of animals with ¹¹C-PIB was limited to 1 h due to the short half-life of the probe (t_{1/2} = 20.4 min). Notably, different distributions in the brain of 6-mo 5xFAD mice were observed using ¹¹C-PIB and ⁶⁴Cu-**9**; the former was identified in plaque with high uptake in the cortex and low accumulations in the hippocampus and the thalamus (29, 69).

The feasibility of early amyloid species detection by PET/CT imaging with ⁶⁴Cu-**9** was studied on 44- to 72-d-old 5xFAD mice. An age-dependent increase in ⁶⁴Cu-**9** uptake (0,236 ± 0,007 vs. 0,310 ± 0,008 %ID/g) was detected in the areas of the thalamus and hippocampus with preference for the former, which has often been overlooked in AD studies (Fig. 5) (68, 70, 71). No accumulation of ⁶⁴Cu-**9** was detected in the cortex of 44-d-old 5xFAD mice; instead, intense PET signal was observed in the pons and medulla (brainstem) of 72-d-old mice, suggesting that Aβ oligomers may spread from the thalamus to other parts of the brain (72). In control experiments, negligible uptake of ⁶⁴Cu-**9** was detected in 44-d-old WT mouse (Fig. 5C). Notably, the uptake of ¹¹C-PIB was measured 40 min post injection on the same ⁶⁴Cu-**9**-imaged 5xFAD mouse taken 3 wk apart and found to be localized at different regions with inferior contrast (Fig. 5B and D). The specific uptake of ⁶⁴Cu-**9** into the brain of young mice relative to ¹¹C-PIB may correlate with levels of Aβ oligomers, which do not bind ¹¹C-PIB. In older mice (95-d-old), ¹¹C-PIB binds preformed fibrils and insoluble plaques located mainly in the cortex, thalamus, and hippocampus correlating with previous studies (73). The observed uptake and localization of ⁶⁴Cu-**9** is an early PET imaging of amyloid species in young presymptomatic transgenic 5xFAD mouse brains.

Postmortem Immunohistochemistry with A11 Antibody Correlates Soluble Aβ Oligomer Locations Identified by PET Imaging with ⁶⁴Cu-9**.** After PET imaging, the 2-mo-old 5xFAD mice were perfused and their brains were sectioned and stained with sequence-specific anti-Aβ 6E10 and oligomer-specific conformational A11 antibodies (Fig. 6). The cortex, subiculum, hippocampus, thalamus, and brainstem, all stained with 6E10 antibody in agreement with previous studies of Aβ localization (68, 72). In contrast, staining with A11 antibody found the highest Aβ oligomer levels in the thalamus followed by the amygdala, hippocampus, and cortex (Fig. 6B–D). The relatively high accumulation of A11-reactive Aβ oligomers in the thalamus correlated with the strong PET signal in this region of the brain indicating detection of Aβ oligomers rather than monomeric or fibrillar Aβ. Fluorescent signals from A11 antibody appeared mainly as punctate structures on intracellular rather than extracellular immunostaining (Fig. 6E) consistent with studies showing that intraneuronal Aβ oligomers are formed in the early stage of the disease and aggregate upon cellular release into intercellular fibrils (68, 74).

Specific Aβ binding was demonstrated in competitive ex vivo binding experiments using azapeptide **7** and a fluorescently labeled

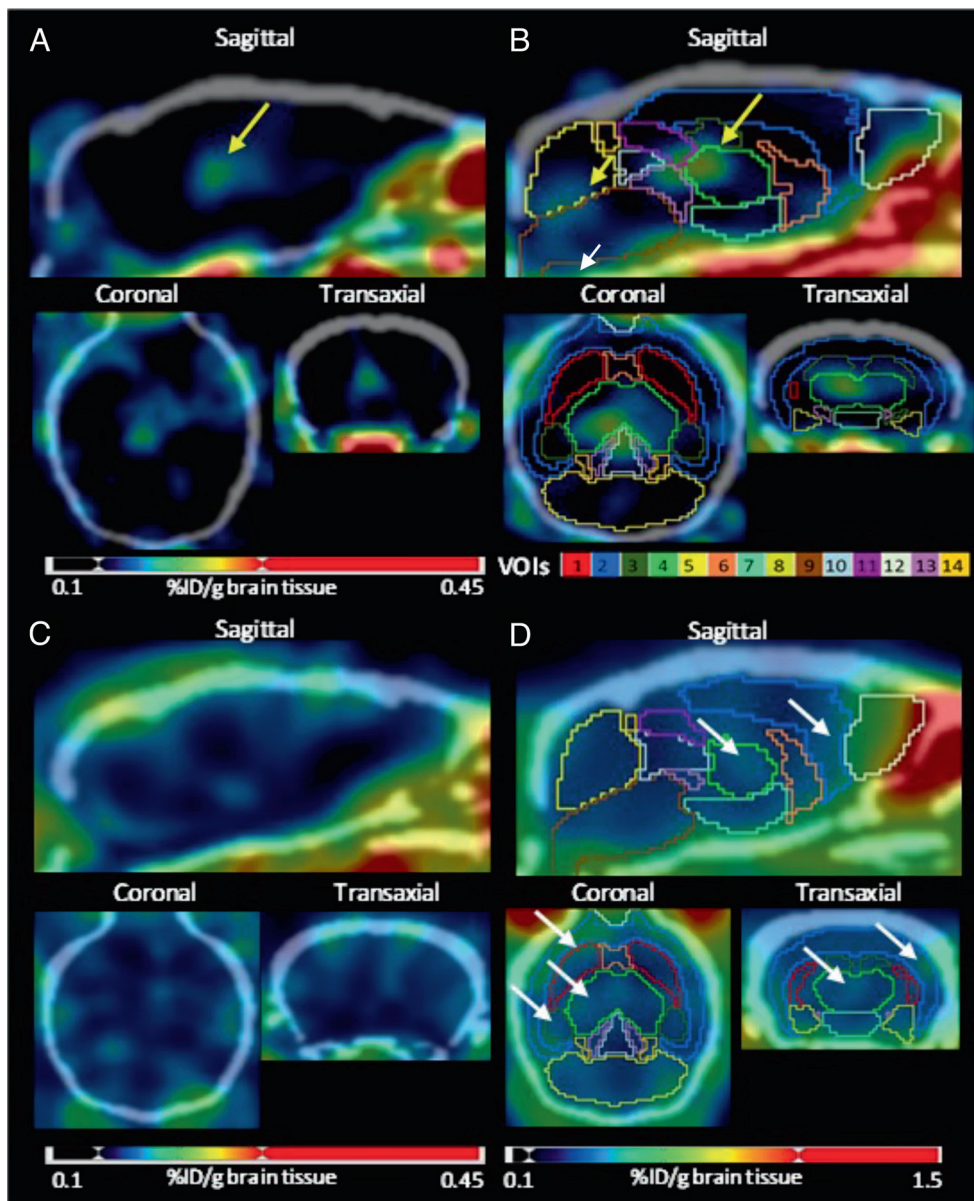


Fig. 5. Representative fused PET-CT images at 1-d postinjection of $^{64}\text{Cu-9}$ into (A) 44-d- and (B) 72-d-old 5xFAD mice ($n = 5$) monitoring progression of $\text{A}\beta$ pathology; (C) 44-d-old WT mice ($n = 3$) at 1-d postinjection of $^{64}\text{Cu-9}$; (D) 40 min postinjection of $^{11}\text{C-PIB}$ into 95-d-old 5xFAD mice ($n = 2$). Red and blue represent, respectively, highest and zero uptake in %ID/g. A different intensity scale was used for PET images (D) with $^{11}\text{C-PIB}$ (0.1–1.5 %ID/g) compared with 0.1–0.45 %ID/g for A, B and C. The yellow arrow points to $\text{A}\beta$ species accumulation in the thalamus. White arrows point to plaque accumulation in the cortex, hippocampus, and thalamus. In (B and D), coregistration of experimental image data with brain mask to identify mouse atlas space volumes of interest (VOI). 1, striatum; 2, cortex; 3, hippocampus; 4, thalamus; 5, cerebellum; 6, basal forebrain septum; 7, hypothalamus; 8, amygdala; 9, brainstem; 10, central gray; 11, superior colliculi; 12, olfactory bulb; 13, midbrain; 14, inferior colliculi.

$\text{A}\beta$ antibody (Alexa647-6E10). Brain slices derived from 7 mo 5xFAD mice were incubated with azapeptide 7 (25 μM) for 4 h prior to incubation with Alexa647-6E10. Significant reduction in fluorescence intensity was observed after preincubation of slices with 7 (*SI Appendix, Fig. S14*), indicating azapeptide competition with 6E10 for $\text{A}\beta$ binding *ex vivo*.

Peptide 1 Improves Memory and Cognition of Transgenic Mice.

Peptide 1, azapeptide 7 and their NOTA conjugates, all permeated the BBB and bound $\text{A}\beta$ oligomers in transgenic 5xFAD mice. Furthermore, (aza)peptides 1 and 7 alleviated AD-associated symptoms in three transgenic *C. elegans* models by reducing amounts of $\text{A}\beta$ oligomers. Peptide 1 was therefore evaluated further for effects on memory and cognition in the AD mouse model. Presymptomatic 45-d-old 5xFAD mice were injected intraperitoneally 3 times per week with peptide 1 (10 mg/kg) for 16 wk. Control 5xFAD and

WT C57BL/6 mice were treated similarly with vehicle. Prolonged administration of peptide 1 (10 mg/kg) had no toxicity on WT mice. At 21 wk of age, 5xFAD mice treated with peptide 1 exhibited similar body weight to that of vehicle treated WT and 5xFAD mice (*SI Appendix, Fig. S15*). The cognition and spatial memory of 5xFAD mice treated with peptide 1 were evaluated in relevant behavior tests and compared with those of control mice. After the behavior tests, mice were sacrificed, and brains were examined immunohistochemically to assess changes in $\text{A}\beta$ levels.

In the open-field test, which examines exploratory activity and anxiety behavior, 5xFAD mice treated with peptide 1 behaved similarly to WT and 5xFAD control mice as reflected in the comparable number of entries to the center of the arena and distances traveled (Fig. 7 A and B). In the novel object recognition test, which judges short-term memory, untreated 5xFAD mice spent less time exploring novel objects relative to familiar ones. In

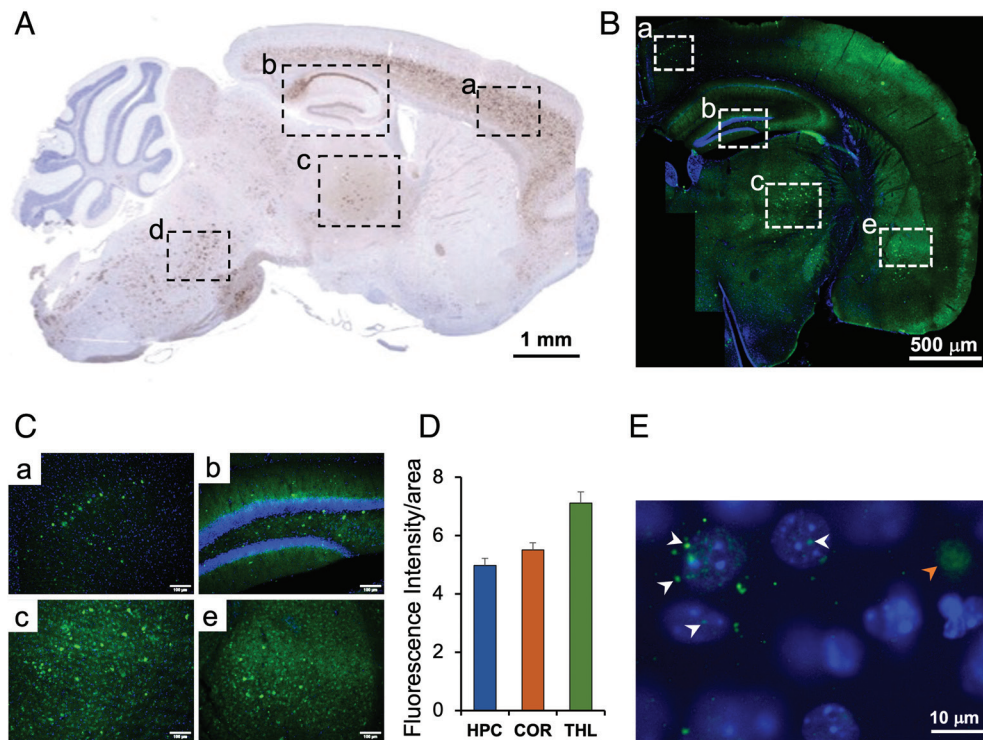


Fig. 6. Immunohistochemical staining of A β species in the 2-mo-old 5xFAD mouse brain. (A) Sagittal section of the 5xFAD mouse brain PET imaged with ^{64}Cu -9 and immunohistochemically examined with sequence-specific 6E10 antibody (recognizing human full-length APP) and developed with anti-mouse horseradish peroxidase (HRP) secondary antibody and 3, 3'-diaminobenzidine (DAB). Positive 6E10 antibody staining was detected in a) cortex, b) hippocampus, c) thalamus and d) pons regions. (B) Representative immunofluorescence image of a coronal section of 2-mo-old 5xFAD mice developed by oligomer-specific A11 antibody and Alexa Fluor 647-labeled secondary antirabbit antibody. Positive A11 antibody staining was detected in the a) cortex, b) hippocampus, c) thalamus, and e) amygdala. (C) Magnified images ($\times 20$) of selected areas in (B). (Scale bars, represent 100 μm .) (D) Quantification of fluorescence intensity of A11-positive A β oligomers obtained from a similar area of the cortex (COR), hippocampus (HPC), and c) thalamus (THL), using ImageJ. (E) Representative immunofluorescence image ($\times 60$) of punctate intracellular (white arrowhead) and extracellular A β oligomers (orange arrowhead) in the thalamus of the 2-mo-old 5xFAD mouse and developed by A11 antibody.

contrast, 5xFAD mice treated with peptide **1** had a similar spontaneous tendency to interact with novel objects as that exhibited by WT mice (Fig. 7C).

Treatment of 5xFAD mice with peptide **1** also improved spatial learning and short-term memory compared with untreated AD mice in the spontaneous alternation Y-maze test (Fig. 7D). The 5xFAD mice exhibited memory deficits and a decreased percentage of spontaneous alternations in the maze. In contrast, AD mice treated with peptide **1** demonstrated a full recovery to levels of WT mice.

In the modified Barnes maze, which tests trial-based learning (75), untreated 5xFAD mice required significantly more time to find the target hole on the sixth day of learning relative to WT mice (Fig. 7E). AD mice treated with peptide **1** required less time and resided in close vicinity to the target hole (Fig. 7E and *SI Appendix*, Fig S16). Moreover, in the spatial memory test at the probe day 7, the treated AD mice behaved indistinguishably from WT mice in searching the target hole (Fig. 7F and G). Collectively, the behavioral tests indicated that prolonged treatment with peptide **1** restored behavior comparable with WT mice and mitigated deficits in cognition, memory and learning which were exhibited by 5xFAD AD mice.

Postmortem Immunohistochemistry Reveals Reduced Levels of A β Species in Brains of 5xFAD Mice Treated with Peptide 1. After behavioral studies, 5xFAD mice were sacrificed and brain slices were examined immunohistochemically using 6E10 antibody to assess effects of peptide **1** on the number of A β species. Significantly lower levels of 6E10-reactive species were observed in the cortex, hippocampus, thalamus, and amygdala regions of the brains of treated 5xFAD mice compared with those of mice treated with vehicle (Fig. 8). The decreased number of A β species in the hippocampus

correlated with significant reduction in A β species in the neurons of the *cornu ammonis* (CA)1 and dentate gyrus (DG), which are associated with learning, cognition, and memory (Fig. 8G and H).

Discussion

Self-assembly and aggregation of pathogenic proteins are associated with more than thirty-five different diseases (3). In AD, soluble aggregates of A β and tau are alleged to be the most toxic species. In recent clinical trials, anti-A β antibodies (e.g., Donanemab, Gantenerumab, and Lecanemab) have cleared amyloid plaques and contributed to slowing cognitive decline and memory loss (18, 76–78). The monoclonal antibody Aduhelm (aducanumab) was granted FDA approval (79). Furthermore, Gantenerumab and Lecanemab were given breakthrough designations to treat AD (80, 81). Controversy over efficacy and notable side effects (e.g., microhemorrhages and brain swelling) (82, 83) highlight needs for better therapy and tools for early AD detection to improve standard of care.

Self-assembled cyclic-D,L- α -peptide nanotubule **1** and amyloid cross- β sheet conformers share similar structural properties responsible for cross-reactivity (33, 34, 38, 41, 84–86). Insertion of an aza-glycine residue into peptide **1** added an extra hydrogen-bond donor, which contingent on location tuned ability for self-assembly into nanotubules as indicated by TEM and DLS experiments (*SI Appendix*, Fig S2). Antiamyloidogenic activity of analogs of peptide **1** correlated with capability to self-assemble (38, 39). Antiamyloidogenic activity increased linearly with augmented hydrophobicity and aromaticity, due likely to enhanced self-assembly. Unprecedented antiamyloidogenic and cytoprotective activities

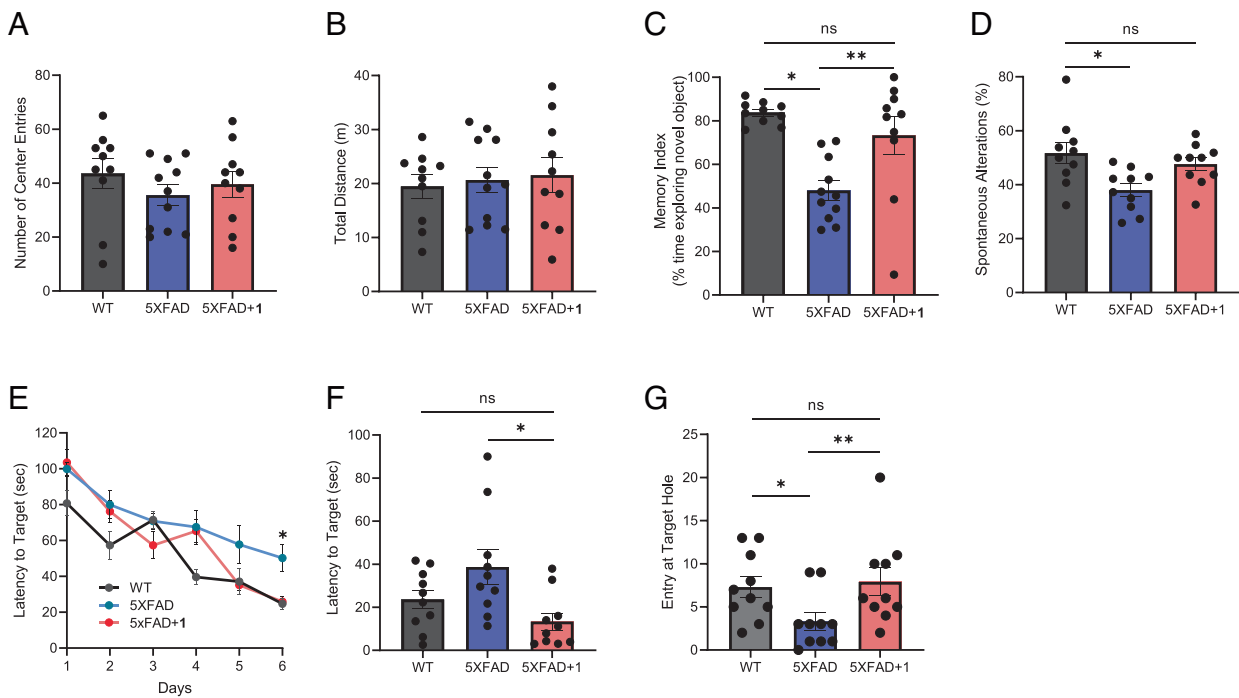


Fig. 7. Effect of chronic treatment with peptide 1 on behavioral activity of 5xFAD mice. (A) Anxiety is measured by the number of entries to the center of the open-field apparatus ($n = 10$, each). (B) Basal locomotor activity of the mice in the open-field test as measured by the total distance traveled by mice. (C) Novel object recognition performance of mice as determined by frequency of novel object exploration. Results represent mean \pm SEM and were analyzed by a one-way ANOVA with Bonferroni's multiple comparison test ($*P < 0.0003$, $**P < 0.0095$, ns = not significant). (D) Increase in spontaneous alterations behavior of 5xFAD mice treated with peptide 1 in the Y-maze test. Mean \pm SEM; a one-way ANOVA followed by Bonferroni's multiple test ($*P < 0.01$, ns=not significant). (E) Latency to reach the target. Learning curve in the Barnes maze from 6 d of spatial learning. Results represent mean \pm SEM and were analyzed by a two-way ANOVA followed by Tukey's multiple comparison test ($*P < 0.0042$). (F) Memory for the target hole on the probe day (day 7) in modified Barnes maze. Transgenic mice show a higher latency time to target, and (G) enter the target hole significantly less often than WT mice ($*P < 0.046$). Treatment of 5xFAD mice with peptide 1 decreased (F) the latency time ($*P < 0.0170$) and (G) increased the number of entries to target hole ($**P < 0.040$). Results in F and G represent mean \pm SEM and were analyzed by the Kruskal-Wallis test.

against A β toxicity, both were exhibited by [azaGly⁶]-1 (7) at sub-stoichiometric concentrations. Peptide 1 and azapeptide 7 also disassembled effectively preformed A β fibrils as indicated by TEM and dot-blotting assays. Certain agents that bind soluble forms of A β , such as antibodies and ECGC have shown ability to interfere with aggregation and to disaggregate preformed fibrils by recycling mechanisms, which shift the equilibrium between fibrillar and soluble forms (46, 48). Azapeptide 7 altered A β conformation and interfered with oligomer and fibril formation as indicated using ThT experiments, CD and NMR spectroscopy, TEM, and immunochemistry. A β oligomer and fibril levels, both were reduced by azapeptide 7. In

the early steps of the proposed mechanism of action, azapeptide 7 complexes F19 and F20 of the K¹⁶LVFF²⁰ aggregation motif. Subsequently, aggregation of A β is shifted away from oligomers and fibrils toward a soluble nontoxic "off-pathway" species.

In established *C. elegans* models of A β 42-induced learning and memory impairments, [azaGly⁶]-1 (7) exhibited preventative effects in vivo. At low concentrations, azapeptide 7 restored WT lifespan and neutralized cognitive and ambulatory impairments due to overexpression of human A β 42 in neuron (CL2355) and muscle (CL2006 and GMC101) tissues in three transgenic *C. elegans* AD models, respectively. Immunochemistry on treated transgenic *C.*

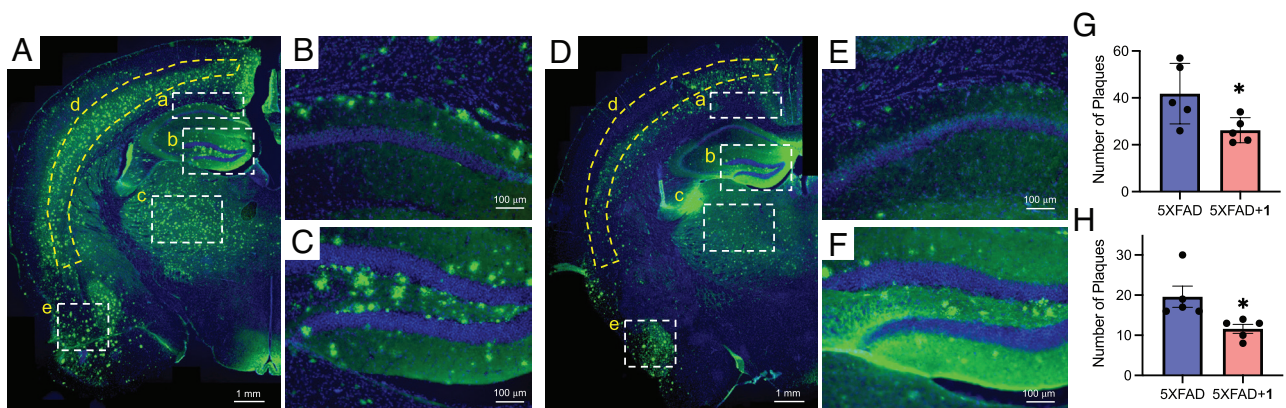


Fig. 8. Effect of treatment with peptide 1 on A β plaque load of 5xFAD mice as determined by IHC using 6E10 antibody. (A, D) Fluorescent images of the brain hemisphere of 5xFAD mice treated with (A) vehicle or (D) peptide 1 for 16 wk. Inserts represent (a) CA1, (b) DG, (c) thalamus, (d) cortex and (e) amygdala. High-magnification images of (B and E) CA1 and (C and F) DG regions. Number of A β plaques per equal area of (G) CA1 and (H) DG. $*P < 0.05$. Data in G and H represent mean \pm SD and were analyzed by a two-tailed *t* test ($n = 5$).

elegans demonstrated that azapeptide **7** decreased effectively both toxic A β oligomers (e.g., hexamers) and plaque levels.

Conjugation to NOTA and radiolabeling of peptide **1** and azapeptide **7** provided, respectively, [Lys¹(⁶⁴Cu/NOTA)]-**1** (⁶⁴Cu-**8**) and [Lys¹(⁶⁴Cu/NOTA), azaGly⁶]-**1** (⁶⁴Cu-**9**) radiotracers for monitoring early AD pathology and progress. Both radiotracers were stable for 24 h in plasma and effectively crossed the BBB. In PET imaging studies of the 44–72-d-old 5xFAD mouse AD model, the distribution of early A β species at various brain regions was studied comprehensively using ⁶⁴Cu-**9**, which demonstrated better accumulation in the brain compared with ⁶⁴Cu-**8**. The relevance of significant quantity of A β oligomer in the thalamus was imaged in young, presymptomatic 5xFAD mice and shown to increase with age, as validated subsequently by immunohistochemistry. Fibrillar A β have been imaged in the thalamus of relatively old 5xFAD mice (5.5–14-mo-old) using the ¹⁸F-PET tracers ¹⁸F-FC119S, ¹⁸F-Florbetapir, and ¹⁸F-Florbetaben (69, 71, 87). In contrast, the PET imaging and immunohistochemistry with oligomer-specific A11 antibody demonstrated that ⁶⁴Cu-**9** gave earlier detection of A β oligomers with superior contrast than ¹¹C-PIB standard, which imaged only late forming plaque in the cortex. Selective binding of A β species in 5xFAD mice was indicated in brain slices using competition experiments between azapeptide **7** and A β -specific 6E10 antibody. Long-term treatment of young presymptomatic 44-d-old 5xFAD mice with peptide **1** for 16 wk reversed safely the cognitive and memory deficits shown in untreated 5xFAD mice by decreasing amyloid aggregates in the hippocampus, thalamus, and cortex.

With potential to modulate the equilibria between self-aggregated and dissociative states of cyclic D,L- α -peptide **1**, azaGly residue substitutions have revealed important insight into the relevance of supramolecular β -sheet interactions for engagement, disruption, and clearance of oligomers. Toward novel agents to diagnose early amyloid diseases for improved treatment, ⁶⁴Cu-**9** represents a promising PET tracer for presymptomatic examination of the emergence and transformation of A β oligomer into plaque. The latter were, respectively, delayed and reduced in transgenic 5xFAD mice by early and prolonged treatment with peptide **1**, which mitigated deficits in cognition, memory, and learning. Further studies are underway to study the exact mode of action of **1** and aza-analogs and to probe the benefits of early diagnosis and the lowering of toxic oligomer levels in the brains of other transgenic mice to alleviate symptoms associated with AD.

Materials and Methods

Synthesis. All six possible [azaGly]-**1** analogs (**2–7**) were made by two different solid-phase approaches from their respective linear precursors (*SI Appendix, Scheme S1*), which were synthesized on 2-chlorotrityl resin, using Fmoc chemistry. The NOTA analogs **8** and **9** were synthesized, respectively, from their precursors **1** and **7**. A β 42 and its isotopically labeled analogs were produced recombinantly in *E. coli*. A more complete description of synthesis, purification, and characterization procedures for azaGly **2–9** and A β analogs are available in *SI Appendix*.

Biophysical and Mechanistic Studies. Effects of peptide analogs **2–9** on A β aggregation were studied by kinetic ThT and TEM, and the mechanism of action

was investigated by CD, DLS, NMR, and dot-blot experiments. Cell culture studies were performed to validate the anti-amyloidogenic activity of the [azaGly]-**1** analogs and to choose the most potent analogs that reduce A β toxicity for further in vivo studies. The design of each study and experimental details are summarized in *SI Appendix*.

In Vivo Efficacy Studies in *C. elegans*. Two transgenic *C. elegans* strains and their respective control strains were used to probe the efficacy of azapeptide **7** on lifespan, locomotion, and chemotaxis behavior of the transgenic worms. The effect of **7** on the amount of A β species in treated worms was then evaluated by immunoblotting techniques. The *C. elegans* strains and the experimental details are available in *SI Appendix*.

In Vivo PET imaging and Efficacy Studies in Mice. Peptides **8** and **9** were radiolabeled with ⁶⁴Cu and their serum binding and stability were determined. The biodistribution of the labeled peptides were studied in normal Balb/c mice. PET imaging with the labeled peptides as well as ¹¹C-PIB was tested in 5xFAD and normal mice. Following the PET imaging, mouse brains were sectioned and subjected to immunochemical studies. For efficacy experiments in mice, wild-type C57BL/6 mice and 5xFAD mice were intraperitoneally injected three times per week for a total duration of 16 wk. For assessment of learning, memory, and cognition, behavior tests such as the modified Barnes maze test, the novel object recognition test, and the spontaneous alternation test were conducted. In addition, basic exploratory activity and anxiety levels were examined by the open-field test. The design of each study and experimental details are summarized in *SI Appendix*.

Statistics. Data were analyzed either by one-way ANOVA, followed by post hoc analysis where appropriate, or by two-tailed, unpaired Student's *t* test if not indicated otherwise, using GraphPad Prism 9 for Mac OS. Statistical details are given in the respective figure legends.

Data, Materials, and Software Availability

All study data are included in the article and/or *SI Appendix*.

ACKNOWLEDGMENTS. We would like to thank Jean-François Beaudoin and Otman Sarrhini from the CIMS/CRCHUS for their support in conducting pre-clinical PET imaging and image data analysis and Dr. Rizwanul Haque from Dr. Oren-Suissa laboratory at the Weizmann Institute of Science for assistance with real-time PCR. The authors acknowledge funding from the MOST-FRONT-FRQS Collaboration in Biomedical Imaging Research, project # 36701 and 3-14012 entitled "Imaging agents for early assessing amyloid disease pathology", and from the Fonds de recherche en santé Québec - Nature et technologies, project # 2021-PR-282135, entitled "Etude des interactions supramoléculaires des feuillettes β pour la détection précoce et la désagrégation des protéines amyloïdes". S.R. also acknowledges partial funding from the Israel Science Foundation (grant No. 2926/21). We thank the Ministère des Relations internationales et de la Francophonie (MRIF) for supporting the project, "Israel-Quebec consortium on early diagnosis and treatment of Alzheimer's disease".

Author affiliations: ^aDepartment of Chemistry, Bar-Ilan University, Ramat-Gan 5290002, Israel; ^bDépartement de Chimie, Université de Montréal, Complexe des Sciences, Québec H2V 0B3, Canada; ^cDepartment of Nuclear Medicine and Radiobiology, Université de Sherbrooke 3001, Sherbrooke, QC J1H 5N4, Canada; ^dSherbrooke Molecular Imaging Center, Research centre of the Centre hospitalier universitaire de Sherbrooke (CHUS), Sherbrooke, QC J1H 5N4, Canada; and ^eThe Leslie and Susan Gonda Multidisciplinary Brain Research Center, the Mina and Everard Goodman Faculty of Life Sciences, and the Paul Feder Laboratory on Alzheimer's Disease Research, Bar-Ilan University, Ramat Gan 5290002, Israel

1. I. W. Hamley, The amyloid beta peptide: A chemist's perspective. Role in Alzheimer's and fibrillization. *Chem. Rev.* **112**, 5147–5192 (2012).
2. P. N. Cheng, J. D. Pham, J. S. Nowick, The supramolecular chemistry of β -sheets. *J. Am. Chem. Soc.* **135**, 5477–5492 (2013).
3. F. Chiti, C. M. Dobson, Protein misfolding, functional amyloid, and human disease. *Annu. Rev. Biochem.* **75**, 333–366 (2006).
4. M. Stefani, C. M. Dobson, Protein aggregation and aggregate toxicity: New insights into protein folding, misfolding diseases and biological evolution. *J. Mol. Med.* **81**, 678–699 (2003).

5. J. Hardy, D. J. Selkoe, The amyloid hypothesis of Alzheimer's disease: Progress and problems on the road to therapeutics. *Science* **297**, 353–356 (2002).
6. Y. H. El-Hayek *et al.*, Tip of the iceberg: Assessing the global socioeconomic costs of Alzheimer's disease and related dementias and strategic implications for stakeholders. *J. Alzheimers Dis.* **70**, 323–341 (2019).
7. C. Haass, D. J. Selkoe, Soluble protein oligomers in neurodegeneration: Lessons from the Alzheimer's amyloid β -peptide. *Nat. Rev. Mol. Cell Biol.* **8**, 101–112 (2007).
8. J. C. Vickers *et al.*, Defining the earliest pathological changes of Alzheimer's disease. *Curr. Alzheimer Res.* **13**, 281–287 (2016).

9. S. Oddo, A. Caccamo, M. Kitazawa, B. P. Tseng, F. M. LaFerla, Amyloid deposition precedes tangle formation in a triple transgenic model of Alzheimer's disease. *Neurobiol. Aging* **24**, 1063–1070 (2003).
10. M. P. Lambert *et al.*, Diffusible, nonfibrillar ligands derived from A β_{1-42} are potent central nervous system neurotoxins. *Proc. Natl. Acad. Sci. U.S.A.* **95**, 6448–6453 (1998).
11. R. M. Koffie *et al.*, Oligomeric amyloid β associates with postsynaptic densities and correlates with excitatory synapse loss near senile plaques. *Proc. Natl. Acad. Sci. U.S.A.* **106**, 4012–4017 (2009).
12. E. N. Cline, M. A. Bicca, K. L. Viola, W. L. Klein, The Amyloid- β oligomer hypothesis: Beginning of the third decade. *J. Alzheimers Dis.* **64**, S567–S610 (2018).
13. M. Fandrich, Oligomeric intermediates in amyloid formation: Structure determination and mechanisms of toxicity. *J. Mol. Biol.* **421**, 427–440 (2012).
14. R. M. Anderson, C. Hadjichrysanthou, S. Evans, M. M. Wong, Why do so many clinical trials of therapies for Alzheimer's disease fail? *Lancet* **390**, 2327–2329 (2017).
15. G. Plascencia-Villa, G. Perry, Status and future directions of clinical trials in Alzheimer's disease. *Int. Rev. Neurobiol.* **154**, 3–50 (2020).
16. J. Sevigny *et al.*, The antibody aducanumab reduces A β plaques in Alzheimer's disease. *Nature* **537**, 50–56 (2016).
17. F. Panza *et al.*, Are antibodies directed against amyloid- β (A β) oligomers the last call for the A β hypothesis of Alzheimer's disease? *Immunotherapy* **11**, 3–6 (2019).
18. C. J. Swanson *et al.*, A randomized, double-blind, phase 2b proof-of-concept clinical trial in early Alzheimer's disease with lecanemab, an anti-A β protofibril antibody. *Alzheimers Res. Ther.* **13**, 80 (2021).
19. T. Bilousova *et al.*, Synaptic amyloid- β oligomers precede p-tau and differentiate high pathology control cases. *Am. J. Pathol.* **186**, 185–198 (2016).
20. F. Zeng *et al.*, Strategies targeting soluble β -Amyloid oligomers and their application to early diagnosis of Alzheimer's disease. *Curr. Alzheimer Res.* **16**, 1132–1142 (2019).
21. R. E. Uhlmann *et al.*, Acute targeting of pre-amyloid seeds in transgenic mice reduces Alzheimer-like pathology later in life. *Nat. Neurosci.* **23**, 1580–1588 (2020).
22. W. M. van Oostveen, E. C. M. de Lange, Imaging techniques in Alzheimer's disease: A review of applications in early diagnosis and longitudinal monitoring. *Int. J. Mol. Sci.* **22**, 2110 (2021).
23. F. Zeng, M. M. Goodman, Fluorine-18 radiolabeled heterocycles as PET tracers for imaging β -amyloid plaques in Alzheimer's disease. *Curr. Top. Med. Chem.* **13**, 909–919 (2013).
24. C. Jie, V. Treyer, R. Schibli, L. Mu, Tauvid: The first FDA-approved PET tracer for imaging tau pathology in Alzheimer's disease. *Pharmaceuticals* **14**, 110 (2021).
25. V. L. Villemagne, V. Dore, S. C. Burnham, C. L. Masters, C. C. Rowe, Imaging tau and amyloid- β proteinopathies in Alzheimer disease and other conditions. *Nat. Rev. Neurol.* **14**, 225–236 (2018).
26. L. Sun *et al.*, Amphiphilic distyrylbenzene derivatives as potential therapeutic and imaging agents for soluble and insoluble amyloid β aggregates in Alzheimer's disease. *J. Am. Chem. Soc.* **143**, 10462–10476 (2021).
27. D. Lee, S. M. Kim, H. Y. Kim, Y. Kim, Fluorescence chemicals to detect insoluble and soluble Amyloid- β aggregates. *ACS Chem. Neurosci.* **10**, 2647–2657 (2019).
28. Y. Zhang, C. Ding, C. Li, X. Wang, Advances in fluorescent probes for detection and imaging of amyloid- β peptides in Alzheimer's disease. *Adv. Clin. Chem.* **103**, 135–190 (2021).
29. D. Sehlin *et al.*, Antibody-based PET imaging of amyloid beta in mouse models of Alzheimer's disease. *Nat. Commun.* **7**, 10759 (2016).
30. S. R. Meier *et al.*, ¹¹C-PIB and ¹²⁴I-antibody PET provide differing estimates of brain amyloid- β after therapeutic intervention. *J. Nucl. Med.* **63**, 302–309 (2021), 10.2967/jnumed.121.262083.
31. M. P. Lambert *et al.*, Monoclonal antibodies that target pathological assemblies of A β . *J. Neurochem.* **100**, 23–35 (2007).
32. K. L. Viola *et al.*, Towards non-invasive diagnostic imaging of early-stage Alzheimer's disease. *Nat. Nanotechnol.* **10**, 91–98 (2015).
33. M. Bucciantini *et al.*, Inherent toxicity of aggregates implies a common mechanism for protein misfolding diseases. *Nature* **416**, 507–511 (2002).
34. R. Kaye *et al.*, Common structure of soluble amyloid oligomers implies common mechanism of pathogenesis. *Science* **300**, 486–489 (2003).
35. M. R. Sawaya *et al.*, Atomic structures of amyloid cross- β spines reveal varied steric zippers. *Nature* **447**, 453–457 (2007).
36. M. I. Ivanova, Y. Lin, Y. H. Lee, J. Zheng, A. Ramamoorthy, Biophysical processes underlying cross-seeding in amyloid aggregation and implications in amyloid pathology. *Biophys. Chem.* **269**, 106507 (2021).
37. M. R. Ghadiri, J. R. Granja, R. A. Milligan, D. E. McRee, N. Khazanovich, Self-assembling organic nanotubes based on a cyclic peptide architecture. *Nature* **366**, 324–327 (1993).
38. M. Richman *et al.*, In vitro and mechanistic studies of an anti-Amyloidogenic self-assembled cyclic D,L- α -peptide architecture. *J. Am. Chem. Soc.* **135**, 3474–3484 (2013).
39. M. Chemerovski-Glikman, M. Richman, S. Rahimpour, Structure-based study of anti-amyloidogenic cyclic D,L- α -peptides. *Tetrahedron* **70**, 7639–7644 (2014).
40. A. Belostozky *et al.*, Inhibition of tau-derived hexapeptide aggregation and toxicity by a self-assembled cyclic D,L- α -peptide conformational inhibitor. *Chem. Commun.* **54**, 5980–5983 (2018).
41. M. Chemerovski-Glikman *et al.*, Self-assembled cyclic D,L- α -peptides as generic conformational inhibitors of the α -synuclein aggregation and toxicity: In vitro and mechanistic studies. *Chemistry* **22**, 14236–14246 (2016).
42. Y. Zhang, R. M. Malamakal, D. M. Chenoweth, Aza-Glycine induces collagen hyperstability. *J. Am. Chem. Soc.* **137**, 12422–12425 (2015).
43. H. LeVine III, Thioflavine T interaction with synthetic Alzheimer's disease β -amyloid peptides: Detection of amyloid aggregation in solution. *Protein Sci.* **2**, 404–410 (1993).
44. G. Bitan *et al.*, Amyloid β -protein (A β) assembly: A β 40 and A β 42 oligomerize through distinct pathways. *Proc. Natl. Acad. Sci. U.S.A.* **100**, 330–335 (2003).
45. S. Lesne *et al.*, A specific amyloid- β protein assembly in the brain impairs memory. *Nature* **440**, 352–357 (2006).
46. J. Bieschke *et al.*, EGCG remodels mature α -synuclein and amyloid- β fibrils and reduces cellular toxicity. *Proc. Natl. Acad. Sci. U.S.A.* **107**, 7710–7715 (2010).
47. K. W. Tipping *et al.*, pH-induced molecular shedding drives the formation of amyloid fibril-derived oligomers. *Proc. Natl. Acad. Sci. U.S.A.* **112**, 5691–5696 (2015).
48. J. McLaurin *et al.*, Therapeutically effective antibodies against amyloid- β peptide target amyloid- β residues 4–10 and inhibit cytotoxicity and fibrillogenesis. *Nat. Med.* **8**, 1263–1269 (2002).
49. A. Bonito-Oliva *et al.*, Conformation-specific antibodies against multiple amyloid protofibril species from a single amyloid immunogen. *J. Cell. Mol. Med.* **23**, 2103–2114 (2019).
50. P. K. Ajikumar, R. Lakshminarayanan, B. T. Ong, S. Valiyaveetil, R. M. Kini, Eggshell matrix protein mimics: Designer peptides to induce the nucleation of calcite crystal aggregates in solution. *Biomacromolecules* **4**, 1321–1326 (2003).
51. M. B. Maina *et al.*, Metal- and UV- catalyzed oxidation results in trapped amyloid- β intermediates revealing that self-assembly is required for A β -induced cytotoxicity. *iScience* **23**, 101537 (2020).
52. E. Gazit, A possible role for pi-stacking in the self-assembly of amyloid fibrils. *FASEB J.* **16**, 77–83 (2002).
53. K. Hochdörfer *et al.*, Rational design of β -sheet ligands against A β_{1-42} -induced toxicity. *J. Am. Chem. Soc.* **133**, 4348–4358 (2011).
54. R. Limbocker *et al.*, Trodusquemine enhances A β_{1-42} aggregation but suppresses its toxicity by displacing oligomers from cell membranes. *Nat. Commun.* **10**, 225 (2019).
55. C. D. Link, Expression of human β -amyloid peptide in transgenic *Caenorhabditis elegans*. *Proc. Natl. Acad. Sci. U.S.A.* **92**, 9368–9372 (1995).
56. Y. Wu *et al.*, Amyloid- β -induced pathological behaviors are suppressed by Ginkgo biloba extract EGB 761 and ginkgolides in transgenic *Caenorhabditis elegans*. *J. Neurosci.* **26**, 13102–13113 (2006).
57. G. McColl *et al.*, Utility of an improved model of amyloid-beta (A β_{1-42}) toxicity in *Caenorhabditis elegans* for drug screening for Alzheimer's disease. *Mol. Neurodegener.* **7**, 57 (2012).
58. O. Hobert, Behavioral plasticity in *C. elegans*: Paradigms, circuits, genes. *J. Neurobiol.* **54**, 203–223 (2003).
59. S. L. Bernstein *et al.*, Amyloid- β protein oligomerization and the importance of tetramers and dodecamers in the aetiology of Alzheimer's disease. *Nat. Chem.* **1**, 326–331 (2009).
60. N. J. Economou *et al.*, Amyloid β -protein assembly and Alzheimer's disease: Dodecamers of A β 42, but not of A β 40, seed fibril formation. *J. Am. Chem. Soc.* **138**, 1772–1775 (2016).
61. N. Osterlund, R. Moons, L. L. Ilag, F. Sobott, A. Gräslund, Native ion mobility-mass spectrometry reveals the formation of β -barrel shaped amyloid- β hexamers in a membrane-mimicking environment. *J. Am. Chem. Soc.* **141**, 10440–10450 (2019).
62. T. D. Do *et al.*, Amyloid β -protein C-terminal fragments: Formation of cylindrins and β -barrels. *J. Am. Chem. Soc.* **138**, 549–557 (2016).
63. A. Aoyagi *et al.*, A β and tau prion-like activities decline with longevity in the Alzheimer's disease human brain. *Sci. Transl. Med.* **11**, eaat8462 (2019).
64. S. Ait-Mohand *et al.*, Evaluation of ⁶⁴Cu-labeled bifunctional chelate-bombesin conjugates. *Bioconjug. Chem.* **22**, 1729–1735 (2011).
65. I. Zawisza, M. Rózga, W. Bał, Affinity of copper and zinc ions to proteins and peptides related to neurodegenerative conditions (A β , APP, α -synuclein, PrP). *Coord. Chem. Rev.* **256**, 2297–2307 (2012).
66. S. Wärmländer *et al.*, Biophysical studies of the amyloid β -peptide: Interactions with metal ions and small molecules. *ChemBiochem* **14**, 1692–1704 (2013).
67. V. Kubicek *et al.*, NOTA complexes with copper(II) and divalent metal ions: Kinetic and thermodynamic studies. *Inorg. Chem.* **57**, 3061–3072 (2018).
68. H. Oakley *et al.*, Intraneuronal β -amyloid aggregates, neurodegeneration, and neuron loss in transgenic mice with five familial Alzheimer's disease mutations: potential factors in amyloid plaque formation. *J. Neurosci.* **26**, 10129–10140 (2006).
69. S. J. Oh *et al.*, Early detection of A β deposition in the 5xFAD mouse by Amyloid PET. *Contrast Media Imaging* **2018**, 5272014 (2018).
70. W. A. Eimer, R. Vassar, Neuron loss in the 5XFAD mouse model of Alzheimer's disease correlates with intraneuronal A β_{42} accumulation and Caspase-3 activation. *Mol. Neurodegener.* **8**, 2 (2013).
71. G. R. Frost *et al.*, Hybrid PET/MRI enables high-spatial resolution, quantitative imaging of amyloid plaques in an Alzheimer's disease mouse model. *Sci. Rep.* **10**, 10379 (2020).
72. A. Ronnback *et al.*, Progressive neuropathology and cognitive decline in a single Arctic APP transgenic mouse model. *Neurobiol. Aging* **32**, 280–292 (2011).
73. S. Rojas *et al.*, In vivo evaluation of amyloid deposition and brain glucose metabolism of 5XFAD mice using positron emission tomography. *Neurobiol. Aging* **34**, 1790–1798 (2013).
74. A. Lord *et al.*, The arctic alzheimer mutation facilitates early intraneuronal A β aggregation and senile plaque formation in transgenic mice. *Neurobiol. Aging* **27**, 67–77 (2006).
75. T. Ilouz, R. Madar, E. Okun, A modified Barnes maze for an accurate assessment of spatial learning in mice. *J. Neurosci. Methods* **334**, 108579 (2020).
76. M. A. Mintun *et al.*, Donanemab in early Alzheimer's disease. *N. Engl. J. Med.* **384**, 1691–1704 (2021).
77. S. Budd Haerlein *et al.*, Two randomized phase 3 studies of aducanumab in early Alzheimer's disease. *J. Prev. Alzheimers Dis.* **9**, 197–210 (2022).
78. S. Salloway *et al.*, A trial of gantenerumab or solanezumab in dominantly inherited Alzheimer's disease. *Nat. Med.* **27**, 1187–1196 (2021).
79. J. Karlawish, J. D. Grill, The approval of Aduhelm risks eroding public trust in Alzheimer research and the FDA. *Nat. Rev. Neurol.* **17**, 523–524 (2021).
80. J. Cummings *et al.*, Alzheimer's disease drug development pipeline: 2022. *Alzheimers Dement. (N.Y.)* **8**, e12295 (2022).
81. N. Villain, V. Planche, R. Levy, High-clearance anti-amyloid immunotherapies in Alzheimer's disease. Part 2: putative scenarios and timeline in case of approval, recommendations for use, implementation, and ethical considerations in France. *Rev. Neurol.* **10**, 1016/j.neuro.2022.08.002 (2022).
82. C. G. Withington, R. S. Turner, Amyloid-related imaging abnormalities with anti-amyloid antibodies for the treatment of dementia due to Alzheimer's Disease. *Front. Neurol.* **13**, 862369 (2022).
83. S. Salloway *et al.*, Amyloid-related imaging abnormalities in 2 phase 3 studies evaluating aducanumab in patients with early Alzheimer disease. *JAMA Neurol.* **79**, 13–21 (2022).
84. M. J. Guerrero-Munoz, D. L. Castillo-Carranza, R. Kaye, Therapeutic approaches against common structural features of toxic oligomers shared by multiple amyloidogenic proteins. *Biochem. Pharmacol.* **88**, 468–478 (2014).
85. J. Luo, S. K. Wärmländer, A. Gräslund, J. P. Abrahams, Cross-interactions between the Alzheimer disease amyloid- β peptide and other amyloid proteins. A further aspect of the amyloid cascade hypothesis. *J. Biol. Chem.* **292**, 2046 (2017).
86. C. Wallin *et al.*, The neuronal tau protein blocks in vitro fibrillation of the amyloid- β (A β) peptide at the oligomeric stage. *J. Am. Chem. Soc.* **140**, 8138–8146 (2018).
87. T. N. Franke *et al.*, In vivo imaging with (18)F-FDG- and (18)F-florbetaben-PET/MRI Detects pathological changes in the brain of the commonly used 5XFAD mouse model of Alzheimer's disease. *Front. Med.* **7**, 529 (2020).